Attitude control strategy for a camera stabilization platform

authored by **F. Königseder, W. Kemmetmüller, and A. Kugi**
and published in *Mechatronics*.

Cite this article as:
F. Königseder, W. Kemmetmüller, and A. Kugi, "Attitude control strategy for a camera stabilization platform", *Mechatronics*, vol. 46, pp. 60–69, 2017. DOI: 10.1016/j.mechatronics.2017.06.012

BibTex entry:

```
% Encoding: UTF-8

@Article{Koenigseder_2017_Mechatronics,
  author = {K\"onigseder, F. and Kemmetm\"uller, W. and Kugi, A.},
  title = {{A}ttitude control strategy for a camera stabilization platform},
  journal = {Mechatronics},
  year = {2017},
  volume = {46},
  pages = {60-69},
  doi = {10.1016/j.mechatronics.2017.06.012},
}

@Comment{jabref-meta: databaseType:bibtex;}
```


Link to original paper:
http://dx.doi.org/10.1016/j.mechatronics.2017.06.012

Contact:

Automation and Control Institute (ACIN)	Internet: www.acin.tuwien.ac.at
Vienna University of Technology	E-mail: office@acin.tuwien.ac.at
Gusshausstrasse 27-29/E376	Phone: +43 1 58801 37601
1040 Vienna, Austria	Fax: +43 1 58801 37699

Attitude control strategy for a camera stabilization platform

Franz Königseder[a], Wolfgang Kemmetmüller[a,*], Andreas Kugi[a]

[a]*Automation and Control Institute, TU Wien, Gusshausstr. 27-29, Vienna, Austria*

Abstract

In this paper, an attitude control strategy for a 3-axis gimbaled platform used for the stabilization of film and broadcast cameras is presented. The attitude control strategy for the camera provides an alignment of the camera's line of sight with a desired attitude, independent of the movements of the platform base. This control objective is achieved by a combination of a feedforward compensation of the disturbances induced by the moving base (the operator) and a feedback control of the orientation of the camera. The required attitude information is obtained by an attitude estimation strategy presented in [1] that fuses the measurements of two inertial measurement units. The derivation of the proposed control law utilizes a number of approximations tailored to the considered application. This allows to obtain an efficient but yet accurate attitude control concept. The very good accuracy and the practical feasibility of the overall control strategy are demonstrated by simulation and measurement results of a prototype platform.

Keywords: attitude control, inertially stabilized platform, camera stabilization

1. Introduction

Camera stabilization is applied in film and broadcast productions to avoid distractions of the line of sight of a dynamically moved camera. A growing use of camera stabilization systems can be observed that goes along with the demand for increasing accuracy and higher flexibility in operation [2, 3]. The main requests are a small and light structure that can be applied in various settings and the capability to turn the camera in any desired direction independently from the motion of the carrier.

Basically, the various approaches for camera stabilization can be divided into passive and active systems. A state-of-the-art passive stabilization of the camera carried by an operator is the steadycam [4]. This system is composed of a pole that has a mount for the camera at the top and counterweights at the bottom. Due to the high inertia of the system and a spring-loaded link to a harness of the operator, the camera is decoupled from the (fast) movements of the operator. Another widespread method for passive camera stabilization is to mount fast rotating momentum wheels to the camera [5].

*Corresponding author

Email addresses: `koenigseder@acin.tuwien.ac.at` (Franz Königseder), `kemmetmueller@acin.tuwien.ac.at` (Wolfgang Kemmetmüller), `kugi@acin.tuwien.ac.at` (Andreas Kugi)

Preprint submitted to Mechatronics *August 23, 2017*

Post-print version of the article: F. Königseder, W. Kemmetmüller, and A. Kugi, "Attitude control strategy for a camera stabilization platform", *Mechatronics*, vol. 46, pp. 60–69, 2017. DOI: 10.1016/j.mechatronics.2017.06.012
The content of this post-print version is identical to the published paper but without the publisher's final layout or copy editing.

Active systems do not have the disadvantage of additionally attached masses and the limited work space due to mechanical constraints. In [6], inertially stabilized platforms (ISPs) are introduced that are typically assembled in the form of actuated gimbals. In the case of three nonparallel joints, the orientation of the camera mounted on an ISP is fully controllable. Since very lightweight constructions exist for these systems, they are often utilized in airborne applications. A system with a double-gimbal is described in [7], which is designed for aerial imaging and visual object tracking. In [8], an inertially stabilized double-gimbal airborne camera platform is presented that is applied to image based pointing and tracking.

Another field of application for ISPs is the stabilization of mobile antennas. Here, the task is to point a mobile vehicle based antenna to a satellite in order to establish a link for data transfer. In [9], a survey of stabilized satcom antenna systems is given and in [10], a ship-mounted satellite tracking antenna is presented.

The sensors used in ISP technology are typically gyroscopes measuring the angular rate in the inertial frame and encoders for position measurement of the joints angles [11]. With these measurements, a control loop for camera stabilization can be applied utilizing a control law of the form [12–14]

$$\boldsymbol{\tau} = \mathbf{K}_v \mathbf{J}^{-1} \Delta\boldsymbol{\omega}, \tag{1}$$

with a positive definite matrix $\mathbf{K}_v$, the manipulator Jacobian $\mathbf{J}$ of the ISP and the error of the angular velocities $\Delta\boldsymbol{\omega}$. This approach can be found in numerous applications because of its simple structure. The drawback of (1) is that it does not provide absolute adjustment of the camera in the inertial frame and it is unfeasible if the manipulator Jacobian $\mathbf{J}$ becomes singular.

The control of the absolute orientation of a body is known as attitude control problem [15] in literature. It is primarily investigated in aerospace applications because of its importance to the navigation of aerial vehicles, see, e.g., [16]. In the attitude control problem, a feedback law of the form

$$\boldsymbol{\tau} = k_p \bar{\mathbf{r}} - k_v \Delta\boldsymbol{\omega}, \tag{2}$$

with the positive scalar controller parameters k_p, k_v, the vector part of a quaternion error $\bar{\mathbf{r}}$ and the error of the angular velocities $\Delta\boldsymbol{\omega}$, is typically utilized. For instance, this approach is applied to a quadcopter in [17]. In [18], a quaternion feedback law for attitude control of a micro satellite is obtained from integrator backstepping. In [19, 20], it is shown how a quaternion feedback controller can be designed without measurements of the angular velocities.

In all contributions of the attitude control problem mentioned so far, the orientation of a single body is stabilized by assuming that the torques acting on the body can be directly applied. In a real stabilization platform, the inertia of the components of the gimbaled platform cannot be neglected such that this assumption is more or less violated. Including the inertia yields a multi-body control task. Up to the authors' knowledge, there is no systematic extension of the attitude control problem (2) to multi-body systems reported in literature and there does not seem to be an application of the attitude control problem to ISPs.

Post-print version of the article: F. Königseder, W. Kemmetmüller, and A. Kugi, "Attitude control strategy for a camera stabilization platform", *Mechatronics*, vol. 46, pp. 60–69, 2017. DOI: 10.1016/j.mechatronics.2017.06.012
The content of this post-print version is identical to the published paper but without the publisher's final layout or copy editing.

According to the classification of control strategies in [21], the control laws (1) and (2) are direct stabilization strategies, which are characterized by utilizing a measurement of the camera's actual movement. In contrast, the indirect stabilization approach achieves stabilization of an ISP by a feedforward compensation of the measured disturbance motion of the ISP base. In [22], the indirect control is applied for stabilizing a manipulator with a forced non-inertial base.

In this paper, a control strategy for the stabilization of a 3-axial ISP is introduced that combines a feedforward compensation of the disturbances with a feedback control of the camera's absolute orientation. The proposed controller constitutes a novel approach to ISP stabilization, which extends the well known position control using inverse dynamics (computed torque), see, e.g., [23, 24].

In Section 2, the platform is introduced and models for the kinematics and dynamics are derived. Moreover, the attitude estimation strategy of [1] is briefly summarized. The derivation of the control strategy is given in Section 3. Section 4 shows the analysis of some specific features of the control strategy by means of simulations. Finally, the control accuracy and the practical feasility of the overall control strategy is analyzed by measurements on a prototype platform in Section 5.

2. System description

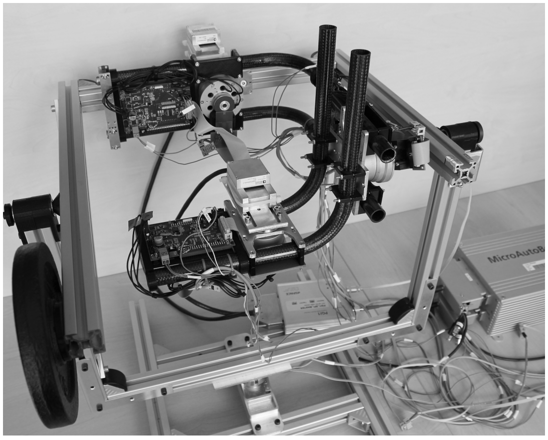

Figure 1: Photo of the prototype platform.

In Fig. 1, a prototype of the platform under consideration is depicted. The sketch of this setup in Fig. 2 shows that the ISP comprises three gimbals p_1, p_2, p_3 and the platform base p_0. The camera is attached to p_3, while the base p_0 is carried by the operator. The bodies p_n, $n = 0, \dots, 3$, are linked by three rotational joints which are actuated by direct-drive brushless dc (BLDC) motors. The joint angles $\mathbf{q} = [q_1, q_2, q_3]^T$ define the actuated degrees of freedom (dof) of the platform. In the experimental setup, the base p_0 of the ISP can be mounted on a suspension, which has the two rotational degrees of freedom ψ and ϕ, see Fig. 2.

Post-print version of the article: F. Königseder, W. Kemmetmüller, and A. Kugi, "Attitude control strategy for a camera stabilization platform", *Mechatronics*, vol. 46, pp. 60–69, 2017. DOI: 10.1016/j.mechatronics.2017.06.012
The content of this post-print version is identical to the published paper but without the publisher's final layout or copy editing.

Each joint is equipped with a high-resolution encoder measuring the actuated dof $\mathbf{q}$ and the disturbance motion represented by ψ and ϕ.

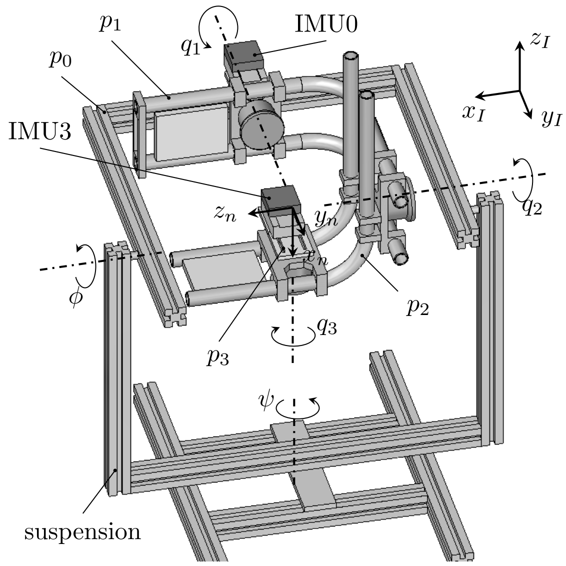

Figure 2: Sketch of the prototype platform.

In real application, the base p_0 is moved by the operator and thus has six dof. Two inertial measurement units (adis 16480 and adis 16485, see [25, 26]) are used to measure the motion of the platform with respect to the inertial frame $(Ix_Iy_Iz_I)$. They provide inertial measurements of the angular velocity and the translational acceleration by means of their integrated 3-axial gyroscope and 3-axial accelerometer. In this paper, a combined feedforward disturbance rejection and feedback control strategy is derived in Section 3. For this task, it proves advantageous to mount an IMU on the base p_0 (IMU0) and one on the position of the camera p_3 (IMU3), see Fig. 2.

2.1. Platform kinematics

According to the model in [1], the inertial orientation of the camera $\mathbf{r}_I^3$ is described by the unit quaternion

$$\mathbf{r}_I^3 = \begin{bmatrix} r_{I,0}^3 \\ r_{I,1}^3 \\ r_{I,2}^3 \\ r_{I,3}^3 \end{bmatrix} = \begin{bmatrix} r_{I,0}^3 \\ \bar{\mathbf{r}}_I^3 \end{bmatrix} = \begin{bmatrix} \cos\left(\frac{\alpha}{2}\right) \\ \mathbf{n}\sin\left(\frac{\alpha}{2}\right) \end{bmatrix}, \tag{3}$$

$\|\mathbf{r}_I^3\|_2 = 1$, which defines the rotation of the body-fixed frame $(3x_3y_3z_3)$ of p_3 with respect to the inertial frame $(Ix_Iy_Iz_I)$, see, e.g., [27, 28] for the basics on quaternion notation. The quaternion $\mathbf{r}_I^3$ is defined by the orientation $\mathbf{r}_I^0$ of the body p_0 with respect to the inertial frame and the relative rotations of the body-fixed

Post-print version of the article: F. Königseder, W. Kemmetmüller, and A. Kugi, “Attitude control strategy for a camera stabilization platform”, *Mechatronics*, vol. 46, pp. 60–69, 2017. DOI: 10.1016/j.mechatronics.2017.06.012
The content of this post-print version is identical to the published paper but without the publisher’s final layout or copy editing.

frames $(nx_ny_nz_n)$, $n = 1, \ldots, 3$, of the three gimbals.

$$\mathbf{r}_2^3 = \left[\cos\left(\tfrac{q_3}{2}\right), \quad \sin\left(\tfrac{q_3}{2}\right), \quad 0, \quad 0\right]^T \tag{4a}$$

$$\mathbf{r}_1^2 = \left[\cos\left(\tfrac{q_2}{2}\right), \quad 0, \quad 0, \quad \sin\left(\tfrac{q_2}{2}\right)\right]^T \tag{4b}$$

$$\mathbf{r}_0^1 = \left[\cos\left(\tfrac{q_1}{2}\right), \quad 0, \quad \sin\left(\tfrac{q_1}{2}\right), \quad 0\right]^T, \tag{4c}$$

the composition of (4) and $\mathbf{r}_I^0$ gives

$$\mathbf{r}_I^3 = \mathbf{r}_I^0 \otimes \mathbf{r}_0^1 \otimes \mathbf{r}_1^2 \otimes \mathbf{r}_2^3 = \mathbf{r}_I^0 \otimes \mathbf{r}_0^3. \tag{5}$$

Therein, $\otimes$ denotes the quaternion product, see, e.g., [27, 28].

The orientation $\mathbf{r}_I^0$ of the base p_0 is defined as

$$\mathbf{r}_I^0 = \begin{bmatrix} \cos\left(\frac{\psi}{2}\right) \\ 0 \\ 0 \\ \sin\left(\frac{\psi}{2}\right) \end{bmatrix} \otimes \begin{bmatrix} \cos\left(\frac{\phi}{2}\right) \\ \sin\left(\frac{\phi}{2}\right) \\ 0 \\ 0 \end{bmatrix} \otimes \begin{bmatrix} \cos\left(\frac{\theta}{2}\right) \\ 0 \\ \sin\left(\frac{\theta}{2}\right) \\ 0 \end{bmatrix}, \tag{6}$$

with the angles ϕ, θ, ψ. In the experimental setup depicted in Fig. 2, the angle θ is fixed to $\theta = \pi/2$. Furthermore, the specific configuration of the platform shown in Fig. 2 is defined by $\mathbf{q} = \mathbf{0}$ and $\psi = \phi = 0$, which yields

$$\mathbf{r}_I^3 = \mathbf{r}_I^0 = \left[\cos(\pi/4), \quad 0, \quad \sin(\pi/4), \quad 0\right]^T. \tag{7}$$

The relative angular velocities are given by

$$\boldsymbol{\omega}_3^{23} = \left[\dot{q}_3, 0, 0\right]^T \tag{8a}$$

$$\boldsymbol{\omega}_2^{12} = \left[0, 0, \dot{q}_2\right]^T \tag{8b}$$

$$\boldsymbol{\omega}_1^{01} = \left[0, \dot{q}_1, 0\right]^T. \tag{8c}$$

Here, the superscript 23 indicates the angular velocity of the body-fixed frame $(3x_3y_3z_3)$ relative to the body-fixed frame $(2x_2y_2z_2)$ expressed in the frame $(3x_3y_3z_3)$ (subscript 3). An analogous notation is utilized for the other quantities in this paper. With (4) and (8), the angular velocity of the camera in the inertial frame can be written as

$$\boldsymbol{\omega}_3^{I3} = \mathbf{R}_3^0 \boldsymbol{\omega}_0^{I0} + \mathbf{R}_3^1 \boldsymbol{\omega}_1^{01} + \mathbf{R}_3^2 \boldsymbol{\omega}_2^{12} + \boldsymbol{\omega}_3^{23}. \tag{9}$$

The rotation matrices $\mathbf{R}_3^n$, $n \in \{I0, 01, 12, 23\}$, are obtained from the corresponding quaternions, see, e.g.,

Post-print version of the article: F. Königseder, W. Kemmetmüller, and A. Kugi, "Attitude control strategy for a camera stabilization platform", *Mechatronics*, vol. 46, pp. 60–69, 2017. DOI: 10.1016/j.mechatronics.2017.06.012
The content of this post-print version is identical to the published paper but without the publisher's final layout or copy editing.

[27, 28]. Finally, the rate of change of the quaternion $\mathbf{r}_I^3$ with respect to time is formulated as

$$\begin{aligned}\dot{\mathbf{r}}_I^3 &= \frac{1}{2}\boldsymbol{\Omega}\left(\omega_3^{I3}\right)\mathbf{r}_I^3 \\ &= \frac{1}{2}\begin{bmatrix} 0 & -\omega_{3,x}^{I3} & -\omega_{3,y}^{I3} & -\omega_{3,z}^{I3} \\ \omega_{3,x}^{I3} & 0 & \omega_{3,z}^{I3} & -\omega_{3,y}^{I3} \\ \omega_{3,y}^{I3} & -\omega_{3,z}^{I3} & 0 & \omega_{3,x}^{I3} \\ \omega_{3,z}^{I3} & \omega_{3,y}^{I3} & -\omega_{3,x}^{I3} & 0 \end{bmatrix}\mathbf{r}_I^3.\end{aligned} \tag{10}$$

In real application, the translational dof of p_0 are defined by the motions of the camera operator. They are described by the vector $\mathbf{p}_I^{I0} = [p_{I,x}^{I0}, p_{I,y}^{I0}, p_{I,z}^{I0}]^T$ from the origin of the inertial frame $(Ix_Iy_Iz_I)$ to the origin of $(0x_0y_0z_0)$ (superscript $I0$) expressed in the inertial frame (subscript I). Since the body-fixed frames $(nx_ny_nz_n)$, $n = 0, 1, 2, 3$ are chosen with coincident origins in the point of intersection of the axes of rotation, $\mathbf{p}_I^{I0} = \mathbf{p}_I^{I1} = \mathbf{p}_I^{I2} = \mathbf{p}_I^{I3}$ holds true, see Fig. 2.

In total, the platform has three actuated dof $\mathbf{q} = [q_1, q_2, q_3]^T$ and six dof defined by the movement of p_0 by the operator. These dof are described in the form $\mathbf{q}_I = [\left(\mathbf{r}_I^0\right)^T, \left(\mathbf{p}_I^{I0}\right)^T]^T \in \mathbb{R}^7$, where the quaternion $\mathbf{r}_I^0$ describes the attitude and $\mathbf{p}_I^{I0}$ is the position with respect to the inertial frame.

2.2. Platform dynamics

For the derivation of the platform dynamics, it is assumed that the attitude and position of the base p_0 described by $\mathbf{q}_I$ is determined by the camera operator and thus is independent of $\mathbf{q}$. Therefore, $\mathbf{q}_I$ can be considered as a time-varying parameter in the subsequent derivations. The equations of motion of the system are derived by the Euler-Lagrange equations, utilizing the kinetic energy T and the potential energy V, see, e.g., [29, 30] for the application to manipulators on a forced non-inertial base. The system's kinetic energy reads as

$$\begin{aligned}T = \frac{1}{2}\sum_{n=1}^{3}\Bigg(& m_n\left(\mathbf{v}_I^{IC_n}\right)^T\mathbf{v}_I^{IC_n} + \\ & \left(\boldsymbol{\omega}_I^{IC_n}\right)^T\mathbf{R}_I^n\mathbf{I}_n\left(\mathbf{R}_I^n\right)^T\boldsymbol{\omega}_I^{IC_n}\Bigg),\end{aligned} \tag{11}$$

with the mass m_n and the moment of inertia $\mathbf{I}_n$ of the body p_n. The angular velocity $\boldsymbol{\omega}_I^{IC_n}$ and the translational velocity $\mathbf{v}_I^{IC_n}$ are defined in the center of gravity C_n of body p_n with respect to the inertial frame $(Ix_Iy_Iz_I)$. They can be expressed with the manipulator Jacobian $\mathbf{J}_I^{IC_n}$ in the form

$$\begin{bmatrix}\boldsymbol{\omega}_I^{IC_n} \\ \mathbf{v}_I^{IC_n}\end{bmatrix} = \mathbf{J}_I^{IC_n}\begin{bmatrix}\dot{\mathbf{q}} \\ \dot{\mathbf{q}}_I\end{bmatrix} = \begin{bmatrix}\mathbf{J}_{I,\omega}^{IC_n} & \mathbf{J}_{I,\omega_I}^{IC_n} \\ \mathbf{J}_{I,v}^{IC_n} & \mathbf{J}_{I,v_I}^{IC_n}\end{bmatrix}\begin{bmatrix}\dot{\mathbf{q}} \\ \dot{\mathbf{q}}_I\end{bmatrix}. \tag{12}$$

Utilizing (12) in (11), the kinetic energy can finally be written as

$$T = \frac{1}{2}\dot{\mathbf{q}}^T\mathbf{D}\dot{\mathbf{q}} + \dot{\mathbf{q}}^T\mathbf{E}\dot{\mathbf{q}}_I + \frac{1}{2}\dot{\mathbf{q}}_I^T\mathbf{F}\dot{\mathbf{q}}_I, \tag{13}$$

Post-print version of the article: F. Königseder, W. Kemmetmüller, and A. Kugi, "Attitude control strategy for a camera stabilization platform", *Mechatronics*, vol. 46, pp. 60–69, 2017. DOI: 10.1016/j.mechatronics.2017.06.012

with

$$
\begin{aligned}
\mathbf{D}(\mathbf{q}) = \sum_{n=1}^{3} \Bigg(& m_n \left(\mathbf{J}_{I,v}^{IC_n}\right)^T \mathbf{J}_{I,v}^{IC_n} + \\
& \left(\mathbf{J}_{I,\omega}^{IC_n}\right)^T \mathbf{R}_I^n \mathbf{I}_n \left(\mathbf{R}_I^n\right)^T \mathbf{J}_{I,\omega}^{IC_n} \Bigg)
\end{aligned} \tag{14a}
$$

$$
\begin{aligned}
\mathbf{E}\left(\mathbf{q}, \mathbf{r}_I^0\right) = \sum_{n=1}^{3} \Bigg(& m_n \left(\mathbf{J}_{I,v}^{IC_n}\right)^T \mathbf{J}_{I,v_I}^{IC_n} + \\
& \left(\mathbf{J}_{I,\omega}^{IC_n}\right)^T \mathbf{R}_I^n \mathbf{I}_n \left(\mathbf{R}_I^n\right)^T \mathbf{J}_{I,\omega_I}^{IC_n} \Bigg)
\end{aligned} \tag{14b}
$$

$$
\begin{aligned}
\mathbf{F}\left(\mathbf{q}, \mathbf{q}_I\right) = \sum_{n=1}^{3} \Bigg(& m_n \left(\mathbf{J}_{I,v_I}^{IC_n}\right)^T \mathbf{J}_{I,v_I}^{IC_n} + \\
& \left(\mathbf{J}_{I,\omega_I}^{IC_n}\right)^T \mathbf{R}_I^n \mathbf{I}_n \left(\mathbf{R}_I^n\right)^T \mathbf{J}_{I,\omega_I}^{IC_n} \Bigg) .
\end{aligned} \tag{14c}
$$

Therein, $\mathbf{J}_{I,v}^{IC_n}$ and $\mathbf{J}_{I,\omega}^{IC_n}$ describe the manipulator Jacobian of the velocity and angular velocity, repectively, of the center of gravity of body n, $n = 1, \ldots, 3$, with relative to the inertial frame. The potential energy is given in the form

$$
V = \sum_{n=1}^{3} \left(m_n \begin{bmatrix} 0, & 0, & g \end{bmatrix} \mathbf{p}_I^{IC_n} \right) , \tag{15}
$$

with the position $\mathbf{p}_I^{IC_n}$ of C_n in the inertial frame and the gravitational acceleration g. The platform dynamics, obtained by the Euler-Lagrange equations, then reads as

$$
\begin{aligned}
\boldsymbol{\tau}_a = & \mathbf{D}(\mathbf{q}) \ddot{\mathbf{q}} + \mathbf{C}(\mathbf{q}, \dot{\mathbf{q}}) \dot{\mathbf{q}} + \mathbf{E}\left(\mathbf{q}, \mathbf{r}_I^0\right) \ddot{\mathbf{q}}_I + \\
& \boldsymbol{\Gamma}\left(\mathbf{q}, \dot{\mathbf{q}}, \mathbf{q}_I, \dot{\mathbf{q}}_I\right) \dot{\mathbf{q}}_I + \mathbf{g}\left(\mathbf{q}, \mathbf{r}_I^0\right) + \boldsymbol{\tau}_f(\dot{\mathbf{q}}) ,
\end{aligned} \tag{16}
$$

with the torques $\boldsymbol{\tau}_a$ of the BLDC motors, the generalized mass matrix $\mathbf{D}(\mathbf{q})$, the Coriolis matrix $\mathbf{C}(\mathbf{q}, \dot{\mathbf{q}})$ and the vector $\mathbf{g}\left(\mathbf{q}, \mathbf{r}_I^0\right)$ of torques due to gravity. The parts $\mathbf{E}\left(\mathbf{q}, \mathbf{r}_I^0\right) \ddot{\mathbf{q}}_I$ and $\boldsymbol{\Gamma}\left(\mathbf{q}, \dot{\mathbf{q}}, \mathbf{q}_I, \dot{\mathbf{q}}_I\right) \dot{\mathbf{q}}_I$ describe the influence of the forced motion of the base.

The friction torque $\boldsymbol{\tau}_f(\dot{\mathbf{q}})$ is mainly caused by the friction in the bearings of the BLDC motors and the joints. This friction is described by a static model of the friction torques $\boldsymbol{\tau}_f = [\tau_{f,1}, \tau_{f,2}, \tau_{f,3}]$ in the form

$$
\tau_{f,n}(\dot{q}_n) = v_n \dot{q}_n + c_n \tanh(\alpha_n \dot{q}_n) , \quad n = 1, 2, 3, \tag{17}
$$

with the viscous friction coefficient v_n and the Coulomb friction coefficient c_n. To obtain a continuous model, the Coulomb friction is approximated by $\tanh(\alpha_n \dot{q}_n)$, where α_n is used to influence the shape of the approximation, see, e.g., [31, 32].

2.3. Inertial measurement

Accurate measurement of the attitude of the platform is decisive for a high control accuracy. In the considered system, two IMUs (IMU0, IMU3) are mounted on the platform, i.e. on p_0 and p_3, respectively.

Post-print version of the article: F. Königseder, W. Kemmetmüller, and A. Kugi, "Attitude control strategy for a camera stabilization platform", *Mechatronics*, vol. 46, pp. 60–69, 2017. DOI: 10.1016/j.mechatronics.2017.06.012
The content of this post-print version is identical to the published paper but without the publisher's final layout or copy editing.

They provide the gyroscope measurements $\tilde{\boldsymbol{\omega}}_n^{In}$ and accelerometer measurements $\tilde{\mathbf{a}}_n^{In}$, $n = 0, 3$. In addition, each actuated dof $\mathbf{q}$ is measured by a high-resolution (18 bit) rotational encoder.

For this platform, an attitude estimation strategy was introduced in [1], which considers the same setup of the platform as in this contribution. The presented attitude estimation strategy utilizes extended und unscented Kalman filtering to calculate the orientation $\hat{\mathbf{r}}_I^0$ by a fusion of the measurements $\tilde{\boldsymbol{\omega}}_n^{In}$, $\tilde{\mathbf{a}}_n^{In}$, $n = 0, 3$. Experimental results show that a very accurate estimation is obtained by the fusion of the measurements of the two IMUs utilizing a tailored multiplicative extended Kalman filter (MEKF). In particular, a significant improvement in comparison to using only a single IMU could be obtained.

The MEKF designed in [1] is utilized in this paper to estimate $\hat{\mathbf{r}}_I^0$ and its time derivative $\dot{\hat{\mathbf{r}}}_I^0$. Furthermore, the orientation of the camera

$$\hat{\mathbf{r}}_I^3 = \hat{\mathbf{r}}_I^0 \otimes \mathbf{r}_0^1(q_1) \otimes \mathbf{r}_1^2(q_2) \otimes \mathbf{r}_2^3(q_3) \tag{18}$$

is obtained by utilizing the encoder measurements $\mathbf{q}$.

The additional measurements of ψ and ϕ of the suspension in the experimental setup are used in Section 3 for the verification of the control accuracy.

3. Control strategy

The control objective is to control the line of sight of the camera described by $\mathbf{r}_I^3$ to a desired orientation $\mathbf{r}_{I,d}^3$,which is defined by the camera operator, e.g., via a joystick, independently of the base motion. For this task, a feedforward compensation of the disturbances is combined with a feedback control of the camera orientation.

3.1. Feedforward compensation

The feedforward compensation part $\boldsymbol{\tau}_a^{ff}$ of the control input aims at compensating all undesired parts in the dynamic model (16). Assuming complete knowledge of the system states and the disturbances, the feedforward part would read as

$$\boldsymbol{\tau}_a^{ff} = \mathbf{C}\dot{\mathbf{q}} + \mathbf{E}\ddot{\mathbf{q}}_I + \boldsymbol{\Gamma}\dot{\mathbf{q}}_I + \mathbf{g} + \boldsymbol{\tau}_f. \tag{19}$$

In practice, however, the orientation $\mathbf{r}_I^0$ and the friction torque $\boldsymbol{\tau}_f$ have to be replaced by their estimated values $\hat{\mathbf{r}}_I^0$ and $\hat{\boldsymbol{\tau}}_f$, respectively. To compensate for $\mathbf{E}\left(\mathbf{q}, \mathbf{r}_I^0\right)\ddot{\mathbf{q}}_I$, exact knowledge of $\ddot{\mathbf{r}}_I^0$ and $\ddot{\mathbf{p}}_I^{I0}$ would be required. While an estimated value of $\ddot{\mathbf{p}}_I^{I0}$ can be obtained by the measured accelerations $\tilde{\mathbf{a}}_0^{I0}$ of IMU0 in the form $\ddot{\mathbf{p}}_I^{I0} \approx \hat{\mathbf{R}}_I^0\tilde{\mathbf{a}}_0^{I0} - \mathbf{g}_I$, it is not possible to obtain a meaningful approximation of $\ddot{\mathbf{r}}_I^0$. Thus,

$$\mathbf{E}\left(\mathbf{q}, \mathbf{r}_I^0\right)\ddot{\mathbf{q}}_I \approx \mathbf{E}_t\left(\mathbf{q}, \hat{\mathbf{r}}_I^0\right)\left(\hat{\mathbf{R}}_I^0\tilde{\mathbf{a}}_0^{I0} - \mathbf{g}_I\right), \tag{20}$$

Post-print version of the article: F. Königseder, W. Kemmetmüller, and A. Kugi, "Attitude control strategy for a camera stabilization platform", *Mechatronics*, vol. 46, pp. 60–69, 2017. DOI: 10.1016/j.mechatronics.2017.06.012
The content of this post-print version is identical to the published paper but without the publisher's final layout or copy editing.

with the vector of gravitation $\mathbf{g}_I = [0, 0, -g]^T$, is used in the feedforward disturbance compensation. Here, $\mathbf{E}_t$ corresponds to the translational part of $\mathbf{E}$. Finally, $\mathbf{C}\dot{\mathbf{q}}$ and $\mathbf{\Gamma}\dot{\mathbf{q}}_I$ are small in comparison to the other terms and can therefore be neglected. Thus, the overall feedforward compensation reads as

$$\boldsymbol{\tau}_a^{ff} = \mathbf{E}_t\left(\mathbf{q}, \hat{\mathbf{r}}_I^0\right)\left(\hat{\mathbf{R}}_I^0 \tilde{\mathbf{a}}_0^{I0} - \mathbf{g}_I\right) + \mathbf{g}\left(\mathbf{q}, \hat{\mathbf{r}}_I^0\right) + \hat{\boldsymbol{\tau}}_f. \tag{21}$$

3.2. Feedback control

In order to stabilize the tracking error in case of model inaccuracies and to reduce the errors due to the simplifications in the feedforward compensation, a feedback control strategy in the form

$$\boldsymbol{\tau}_a^{fb} = \mathbf{D}\left(\mathbf{q}\right)\left(-\mathbf{\Lambda}_1 \dot{\mathbf{e}}_q - \mathbf{\Lambda}_0 \mathbf{e}_q\right), \tag{22}$$

with the tracking error $\mathbf{e}_q = \mathbf{q} - \mathbf{q}_d$, its time derivative $\dot{\mathbf{e}}_q$ and the positive definite diagonal matrices $\mathbf{\Lambda}_1$, $\mathbf{\Lambda}_0$, is used.

This formulation of the feedback control law has the drawback that for determining the desired orientation $\mathbf{q}_d$ the inverse kinematics has to be calculated, which is rather complex. More important, the main control task is to stabilize the camera, i.e. to control the platform such that the actual camera orientation $\mathbf{r}_I^3$ is equal to the desired orientation $\mathbf{r}_{I,d}^3$. Thus, feedback of the error $\mathbf{e}_r = \hat{\mathbf{r}}_I^3 - \mathbf{r}_{I,d}^3$ between the measured and the desired orientation is more meaningful.

The camera orientation $\mathbf{r}_I^3$ is given by the nonlinear relation between the actuated degrees of freedom $\mathbf{q}$ and the orientation $\mathbf{r}_I^0$ of the handle in the form

$$\mathbf{r}_I^3 = \mathbf{r}_I^0 \otimes \mathbf{r}_0^3 = \mathbf{f}_c\left(\mathbf{q}, \mathbf{r}_I^0\right). \tag{23}$$

Accordingly, the desired camera orientation can be written in the form $\mathbf{r}_{I,d}^3 = \mathbf{f}_c\left(\mathbf{q}_d, \mathbf{r}_I^0\right)$. Assuming small errors $\mathbf{e}_q$, the following approximation holds

$$\mathbf{r}_{I,d}^3 \approx \mathbf{f}_c\left(\mathbf{q}, \mathbf{r}_I^0\right) - \underbrace{\frac{\partial \mathbf{f}_c}{\partial \mathbf{q}}\left(\mathbf{q}, \mathbf{r}_I^0\right)}_{\mathbf{J}_r\left(\mathbf{q}, \mathbf{r}_I^0\right)} \mathbf{e}_q, \tag{24}$$

where $\mathbf{J}_r$ denotes the Jacobian of $\mathbf{f}_c$ with respect to $\mathbf{q}$. With this result, the camera orientation error $\mathbf{e}_r = \mathbf{r}_I^3 - \mathbf{r}_{I,d}^3$ is related to $\mathbf{e}_q$ in the form

$$\mathbf{e}_r = \mathbf{J}_r\left(\mathbf{q}, \mathbf{r}_I^0\right)\mathbf{e}_q. \tag{25}$$

The corresponding time derivatives of the actual and desired camera orientation read as

$$\dot{\mathbf{r}}_I^3 = \frac{\partial \mathbf{f}_c}{\partial \mathbf{q}}\left(\mathbf{q}, \mathbf{r}_I^0\right)\dot{\mathbf{q}} + \frac{\partial \mathbf{f}_c}{\partial \mathbf{r}_I^0}\left(\mathbf{q}, \mathbf{r}_I^0\right)\dot{\mathbf{r}}_I^0 \tag{26a}$$

$$\dot{\mathbf{r}}_{I,d}^3 = \frac{\partial \mathbf{f}_c}{\partial \mathbf{q}}\left(\mathbf{q}_d, \mathbf{r}_I^0\right)\dot{\mathbf{q}}_d + \frac{\partial \mathbf{f}_c}{\partial \mathbf{r}_I^0}\left(\mathbf{q}_d, \mathbf{r}_I^0\right)\dot{\mathbf{r}}_I^0. \tag{26b}$$

Post-print version of the article: F. Königseder, W. Kemmetmüller, and A. Kugi, "Attitude control strategy for a camera stabilization platform", *Mechatronics*, vol. 46, pp. 60–69, 2017. DOI: 10.1016/j.mechatronics.2017.06.012
The content of this post-print version is identical to the published paper but without the publisher's final layout or copy editing.

Assuming again a small error $\mathbf{e}_q$, the approximations $\mathbf{J}_r\left(\mathbf{q},\mathbf{r}_I^0\right) \approx \mathbf{J}_r\left(\mathbf{q}_d,\mathbf{r}_I^0\right)$ and

$$\frac{\partial \mathbf{f}_c}{\partial \mathbf{r}_I^0}\left(\mathbf{q},\mathbf{r}_I^0\right) \approx \frac{\partial \mathbf{f}_c}{\partial \mathbf{r}_I^0}\left(\mathbf{q}_d,\mathbf{r}_I^0\right) \tag{27}$$

are feasible and thus

$$\dot{\mathbf{e}}_r = \mathbf{J}_r\left(\mathbf{q},\mathbf{r}_I^0\right)\dot{\mathbf{e}}_q \tag{28}$$

holds.

Remark 1. *The Jacobian $\mathbf{J}_r$ has independent columns in every configuration $\mathbf{q}$ except for the singular configuration, which occurs for $q_2 = \pm\pi/2$. The singular configuration is, however, not admissible in the real setup and thus irrelevant for the practical operation.*

Given the Jacobian $\mathbf{J}_r$ with full column rank, the following result is obtained from (25) and (28)

$$\mathbf{e}_q = \left(\mathbf{J}_r^T\mathbf{J}_r\right)^{-1}\mathbf{J}_r^T\mathbf{e}_r = \mathbf{A}\mathbf{e}_r \tag{29a}$$

$$\dot{\mathbf{e}}_q = \left(\mathbf{J}_r^T\mathbf{J}_r\right)^{-1}\mathbf{J}_r^T\dot{\mathbf{e}}_r = \mathbf{A}\dot{\mathbf{e}}_r. \tag{29b}$$

The overall control input $\boldsymbol{\tau}_a$ is finally given in the form $\boldsymbol{\tau}_a = \boldsymbol{\tau}_a^{ff} + \boldsymbol{\tau}_a^{fb}$, with $\boldsymbol{\tau}_a^{ff}$ and $\boldsymbol{\tau}_a^{fb}$ from (21) and (22), respectively. Note that in the real application, the quaternions $\mathbf{r}_I^0$ and $\mathbf{r}_I^3$ are replaced by their estimated values $\hat{\mathbf{r}}_I^0$ and $\hat{\mathbf{r}}_I^3$, respectively. Figure 3 depicts the scheme of the overall control strategy.

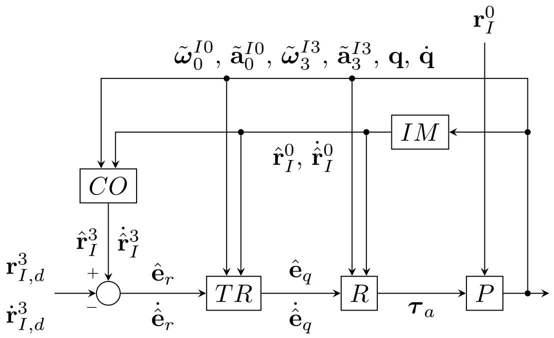

Figure 3: Scheme of the overall control strategy, composed of the estimation of the camera orientation CO, the inertial measurement IM, transformation of the control error TR according to (25) and (28), the controller R according to (21) and (22), and the camera stabilization platform P.

Remark 2. *Using the control law* (21), (22) *in* (16)*, the dynamics of the closed-loop system can be written in the form*

$$\mathbf{D}(\mathbf{q})\left(\ddot{\mathbf{e}}_q + \boldsymbol{\Lambda}_1\dot{\mathbf{e}}_q + \boldsymbol{\Lambda}_0\mathbf{e}_q\right) = \boldsymbol{\eta} \tag{30}$$

Post-print version of the article: F. Königseder, W. Kemmetmüller, and A. Kugi, "Attitude control strategy for a camera stabilization platform", *Mechatronics*, vol. 46, pp. 60–69, 2017. DOI: 10.1016/j.mechatronics.2017.06.012

with

$$\begin{aligned}\boldsymbol{\eta} = -\mathbf{D}(\mathbf{q})\ddot{\mathbf{q}}_d - \mathbf{C}(\mathbf{q},\dot{\mathbf{q}})\dot{\mathbf{q}} - \boldsymbol{\Gamma}(\mathbf{q},\dot{\mathbf{q}},\mathbf{q}_I,\dot{\mathbf{q}}_I)\dot{\mathbf{q}}_I - \\ \mathbf{E}\left(\mathbf{q},\mathbf{r}_I^0\right)\ddot{\mathbf{q}}_I + \mathbf{g}\left(\mathbf{q},\hat{\mathbf{r}}_I^0\right) - \mathbf{g}\left(\mathbf{q},\mathbf{r}_I^0\right) + \\ \mathbf{E}_t\left(\mathbf{q},\hat{\mathbf{r}}_I^0\right)\left(\hat{\mathbf{R}}_I^0\tilde{\mathbf{a}}_0^{I0} - \mathbf{g}_I\right) + \hat{\boldsymbol{\tau}}_f - \boldsymbol{\tau}_f.\end{aligned} \tag{31}$$

Clearly, the closed-loop system (30) *is exponentially stable for* $\boldsymbol{\eta} = \mathbf{0}$ *and positive definite diagonal matrices* $\boldsymbol{\Lambda}_1$ *and* $\boldsymbol{\Lambda}_0$*. Further,* $\boldsymbol{\eta}$ *is bounded if* $\ddot{\mathbf{r}}_I^0$, $\ddot{\mathbf{p}}_I^{I0}$ *are bounded and the terms* $\mathbf{C}\dot{\mathbf{q}}$, $\boldsymbol{\Gamma}\dot{\mathbf{q}}_I$ *are small in the considered application. Following the lines of [33–36], also boundedness of* $\mathbf{e}_q$ *can be concluded.*

4. Simulation results

In this section, simulation results of the proposed attitude control strategy for the camera stabilization platform are presented. The main objective of the simulations is to evaluate the simplifications made in the controller design and their influence on the control accuracy. Thus, an ideal actuation of the platform, ideal sensors and the exact knowledge of the orientations $\mathbf{r}_I^0$, $\mathbf{r}_I^3$ are assumed, i.e., inaccuracies due to erroneous estimations $\hat{\mathbf{r}}_I^0$ and $\hat{\mathbf{r}}_I^3$ are not considered. The practical feasibility of the proposed control concept will be studied later by measurement results, which, as a matter of fact, incorporate all these neglected effects.

The simulation model in MATLAB/SIMULINK covers the control law (21), (22) and the complete equations of motion (16). The parameters of the platform are given by geometry and material data and are identified for the prototype platform shown in Fig. 1. The main system parameters, including the camera mounted on p_3, are summarized in Table 1. The controller parameters are chosen to $\boldsymbol{\Lambda}_0 = \mathrm{diag}\,[10, 10, 10]$ and $\boldsymbol{\Lambda}_1 = \mathrm{diag}\,[0.13, 0.13, 0.13]$, and the controller is implemented with a sampling time $T_s = 1\,\mathrm{ms}$.

object	mass	length	width	height
p_1	1.513 kg	335 mm	320 mm	120 mm
p_2	0.726 kg	267 mm	120 mm	335 mm
p_3	0.183 kg	250 mm	100 mm	106 mm
camera	2.2 kg	230 mm	100 mm	100 mm

Table 1: Geometrical and mechanical parameters of the prototype platform and the camera mounted on p_3.

The inputs of the simulations are the forced dof $\mathbf{q}_I$ and the desired orientation $\mathbf{r}_{I,d}^3$ of the camera. In the simulations, a combined change of the orientation $\mathbf{r}_I^0$ and the position $\mathbf{p}_I^{I0}$, as well as of the desired orientation $\mathbf{r}_{I,d}^3$ is examined. Fig. 4 shows the corresponding simulation inputs, where in Fig. 4a), the parameterizing angles ϕ, θ and ψ of $\mathbf{r}_I^0$ are depicted, cf. (6). Furthermore, the desired orientation $\mathbf{r}_{I,d}^3$ is obtained from the desired angular speed $\omega_{3,d}^{I3}$ given in Fig. 4d). Note that the chosen motion of the forced dof is in the range of the fastest motions, which can be expected in the real application.

Post-print version of the article: F. Königseder, W. Kemmetmüller, and A. Kugi, "Attitude control strategy for a camera stabilization platform", *Mechatronics*, vol. 46, pp. 60–69, 2017. DOI: 10.1016/j.mechatronics.2017.06.012

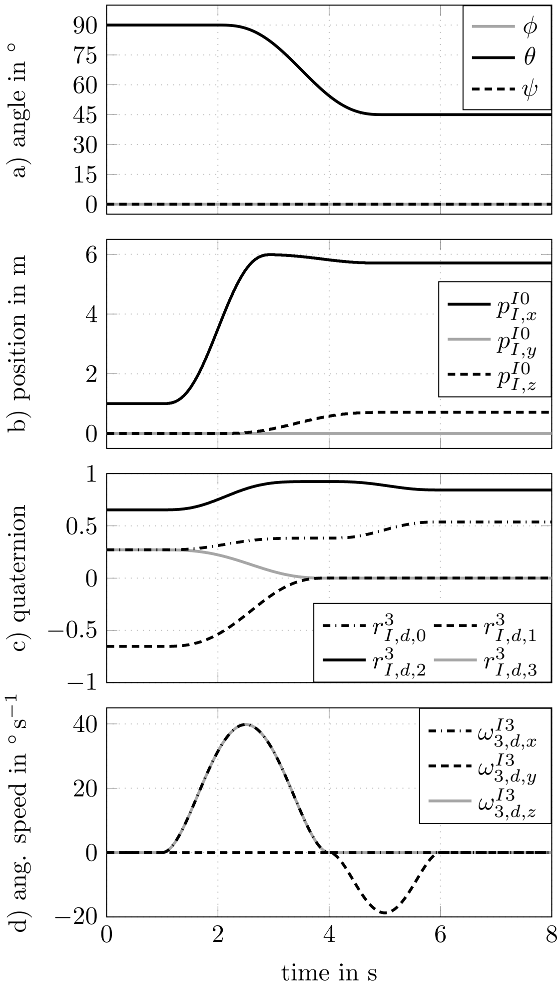

Figure 4: Simulation inputs: a-b) rotation and translation of body p_0, c-d) desired orientation $\mathbf{r}^{3}_{I,d}$ and angular speed $\boldsymbol{\omega}^{I3}_{3,d}$ of body p_3.

Post-print version of the article: F. Königseder, W. Kemmetmüller, and A. Kugi, "Attitude control strategy for a camera stabilization platform", *Mechatronics*, vol. 46, pp. 60–69, 2017. DOI: 10.1016/j.mechatronics.2017.06.012

The resulting actuated dof $\mathbf{q}$ are depicted in Fig. 5 together with the control error $\mathbf{e}_r$. Since an evaluation of the control accuracy based on quaternions and $\mathbf{e}_r$ is rather difficult, Fig. 5 additionally shows the errors in the angles α, β and γ which parameterize the orientation $\mathbf{r}_I^3$ of the camera in the form

$$\mathbf{r}_I^3 = \begin{bmatrix} \cos\left(\frac{\alpha}{2}\right) \\ 0 \\ \sin\left(\frac{\alpha}{2}\right) \\ 0 \end{bmatrix} \otimes \begin{bmatrix} \cos\left(\frac{\beta}{2}\right) \\ 0 \\ 0 \\ \sin\left(\frac{\beta}{2}\right) \end{bmatrix} \otimes \begin{bmatrix} \cos\left(\frac{\gamma}{2}\right) \\ \sin\left(\frac{\gamma}{2}\right) \\ 0 \\ 0 \end{bmatrix}. \tag{32}$$

Therein, the angles α, β and γ are calculated by the inverse kinematics analogously to [37]. It can be seen from this plot that a very high tracking control accuracy in the range $\pm 0.3°$ is obtained in this idealized simulation scenario. The plots of the errors in the angular velocities $\boldsymbol{\omega}_{3,d}^{I3} - \boldsymbol{\omega}_3^{I3}$ confirm this result and further show a rather smooth tracking without introducing undesired vibrations.

The control input $\boldsymbol{\tau}_a$ is presented in Fig. 6a). The feedforward part $\boldsymbol{\tau}_a^{ff}$ of the control input (21) can be split into $\boldsymbol{\tau}_a^{ff} = \boldsymbol{\tau}_e + \boldsymbol{\tau}_g + \hat{\boldsymbol{\tau}}_f$, with $\boldsymbol{\tau}_e = \mathbf{E}_t \left(\hat{\mathbf{R}}_I^0 \tilde{\mathbf{a}}_0^{I0} - \mathbf{g}_I \right)$, $\boldsymbol{\tau}_g = \mathbf{g}$ and the estimated friction torques $\hat{\boldsymbol{\tau}}_f$. It is evident from Fig. 6b-d) that the gravitational part $\boldsymbol{\tau}_g$ and the dynamic part $\boldsymbol{\tau}_e$ are considerably larger than the friction torque $\hat{\boldsymbol{\tau}}_f$. Note that this low level of friction is obtained by using direct drive brushless dc-motors for the actuation of the platform.

The feedback control part $\boldsymbol{\tau}_a^{fb}$ allows to draw conclusions on the feasibility of the approximations which were used in the derivation of the feedforward control strategy, i.e. on the size of $\boldsymbol{\eta}$ in (31). It can easily be seen from Fig. 6e) that only a rather small control input is necessary to cope with these errors. This allows to conclude that the simplifications made during the controller design are practically feasible and only have a minor influence on the closed-loop system.

To analyze the benefit of utilizing the nonlinear feedforward part $\boldsymbol{\tau}_a^{ff}$ according to (21), the control strategy with feedback control part only (i.e. $\boldsymbol{\tau}_a^{ff} = \mathbf{0}$) is simulated for the same simulation inputs as given in Fig. 4. The results depicted in Fig. 7a) show a drastically increased attitude error, which clearly indicates the advantage of utilizing the proposed feedforward part. While it would be theoretically possible to decrease the error by increasing the controller parameters $\boldsymbol{\Lambda}_1$ and $\boldsymbol{\Lambda}_0$, this would also increase the influence of measurement noise and thus is not feasible for practical application.

In a further simulation, the behavior of a conventional control strategy similar to (1) in the form $\boldsymbol{\tau}_a^{fb} = \boldsymbol{\Lambda}_1 \mathbf{J}_{3,\omega}^{0C_3} \left(\boldsymbol{\omega}_{3,d}^{I3} - \boldsymbol{\omega}_3^{I3} \right)$ is utilized instead of (22), where $\mathbf{J}_{3,\omega}^{0C_3}$ is the manipulator Jacobian of the angular velocity of C_3 relative to the body 0, described in the body-fixed frame $(3x_3y_3z_3)$. Since the last simulation already showed that neglecting the feedforward part $\boldsymbol{\tau}_a^{ff}$ drastically decreases the control performance, this conventional feedback strategy is combined with the feedforward control strategy (21). Fig. 7b) shows the control accuracy for this case, where the controller parameter $\boldsymbol{\Lambda}_1$ is chosen approximately 20 times the value utilized for the proposed feedback control (22). Even for this rather large value, which will not be feasible

Post-print version of the article: F. Königseder, W. Kemmetmüller, and A. Kugi, "Attitude control strategy for a camera stabilization platform", *Mechatronics*, vol. 46, pp. 60–69, 2017. DOI: 10.1016/j.mechatronics.2017.06.012
The content of this post-print version is identical to the published paper but without the publisher's final layout or copy editing.

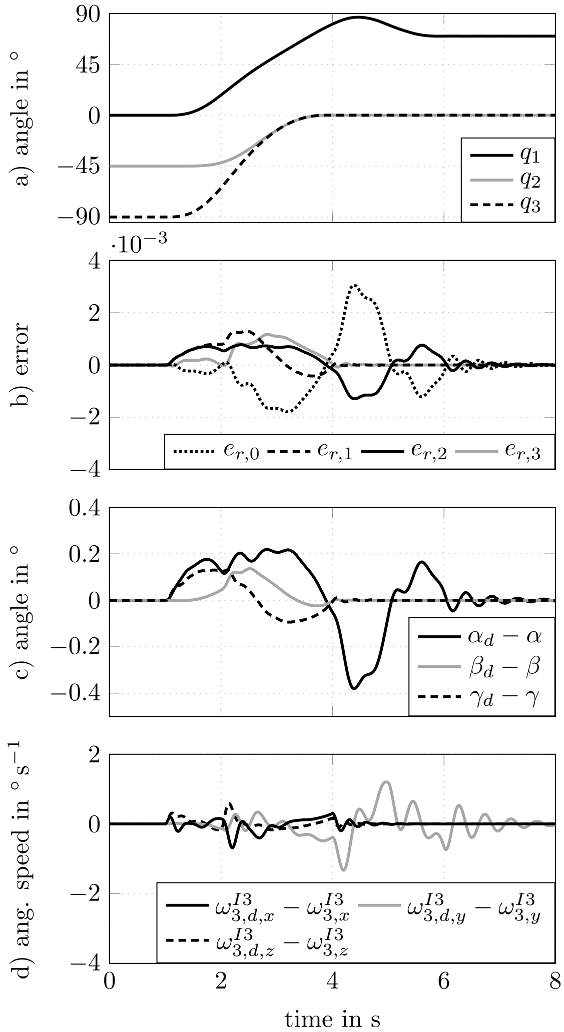

Figure 5: Simulation results: a) actuated dof $\mathbf{q}$, b) orientation error $\mathbf{e}_r$, c) corresponding error in the angles and, d) error in the angular velocity $\boldsymbol{\omega}^{I3}_{3,d} - \boldsymbol{\omega}^{I3}_{3}$.

Post-print version of the article: F. Königseder, W. Kemmetmüller, and A. Kugi, "Attitude control strategy for a camera stabilization platform", *Mechatronics*, vol. 46, pp. 60–69, 2017. DOI: 10.1016/j.mechatronics.2017.06.012
The content of this post-print version is identical to the published paper but without the publisher's final layout or copy editing.

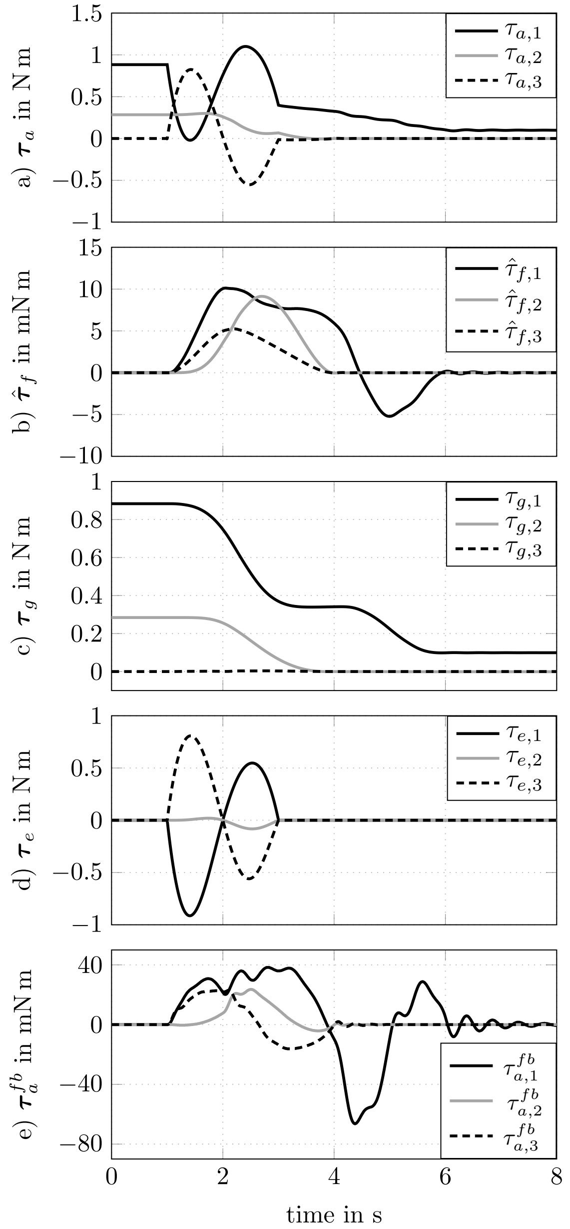

Figure 6: Simulation results: a) overall control input $\boldsymbol{\tau}_a$, b-d) parts of the feedforward control input $\boldsymbol{\tau}_a^{ff}$, see (21), and e) feedback control input $\boldsymbol{\tau}_a^{fb}$. Please note the different scaling of the y-axis.

Post-print version of the article: F. Königseder, W. Kemmetmüller, and A. Kugi, "Attitude control strategy for a camera stabilization platform", *Mechatronics*, vol. 46, pp. 60–69, 2017. DOI: 10.1016/j.mechatronics.2017.06.012
The content of this post-print version is identical to the published paper but without the publisher's final layout or copy editing.

for practical application due to the resulting amplification of measurement noise, the conventional feedback control strategy is clearly outperformed by the proposed feedback control strategy.

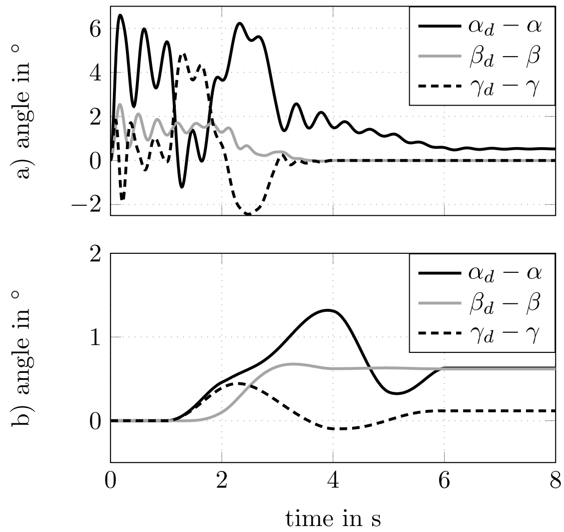

Figure 7: Simulation results: a) control accuracy without feedforward part $\boldsymbol{\tau}_a^{ff} = \mathbf{0}$ and b) control accuracy for conventional feedback strategy.

The proposed control strategy is based on the mathematical model of the system and assumes accurate knowledge of the system parameters. In real application, in particular the mounting position (center of gravity) and the mass of the camera might not be perfectly known. Simulation results with an assumed maximum error of 10% in both the position and mass of the camera proved the robust stability of the proposed control strategy. The control accuracy, however, is slightly decreased with a maximum error of approximately $\pm 1°$ for a similar experiment as in Fig. 4. Further analysis shows that the main reason for the reduced control accuracy are the errors in the mounting position of the camera in the center of gravity. This parameter error could be reduced by a calibration, e.g., by identifying the center of gravity of the camera.

5. Measurement results

While the simulation results allow systematical analysis of the influence of the simplifications made in the course of the controller design, the practical feasibility is proven by measurements on the experimental setup depicted in Fig. 1. As described in Section 2, the setup comprises the fully actuated platform and the suspension. An electronic control unit (dSPACE DS1401) is utilized to evaluate the sensor data and to calculate the attitude estimation algorithm of [1] and the control law (21), (22) at a sampling time of 1 ms. A power electronics unit is provided for each BLDC motor, which utilizes field-oriented torque control to realize the torque $\boldsymbol{\tau}_a$ of the attitude control strategy.

Post-print version of the article: F. Königseder, W. Kemmetmüller, and A. Kugi, "Attitude control strategy for a camera stabilization platform", *Mechatronics*, vol. 46, pp. 60–69, 2017. DOI: 10.1016/j.mechatronics.2017.06.012

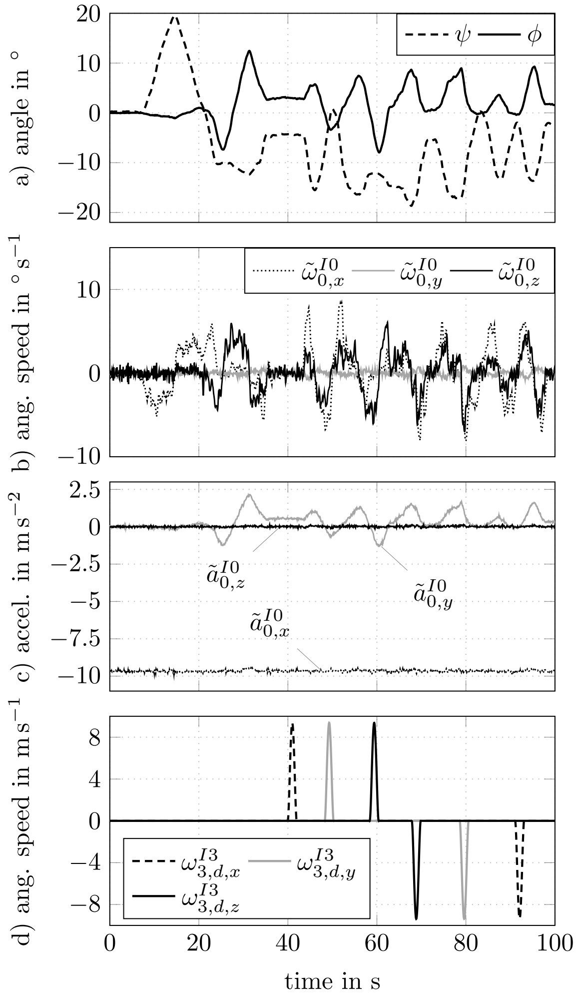

Figure 8: Experimental results: a) encoder measurements ϕ and ψ of the gimbal, b-c) measurements $\tilde{\boldsymbol{\omega}}_0^{I0}$ and $\tilde{\mathbf{a}}_0^{I0}$ of IMU0 and, d) desired angular speed $\boldsymbol{\omega}_{3,d}^{I3}$ of body p_3 (camera).

Post-print version of the article: F. Königseder, W. Kemmetmüller, and A. Kugi, "Attitude control strategy for a camera stabilization platform", *Mechatronics*, vol. 46, pp. 60–69, 2017. DOI: 10.1016/j.mechatronics.2017.06.012

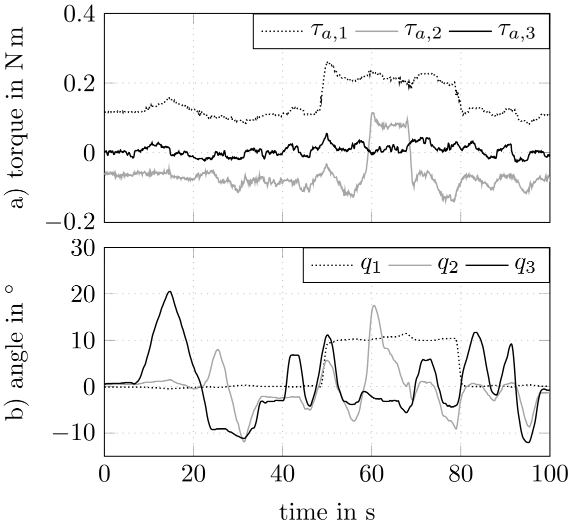

Figure 9: Experimental results: a) torques $\boldsymbol{\tau}_a$ and, b) orientation $\mathbf{q}$ of the actuated dof.

In the present experiment, the camera operator defines the desired orientation $\mathbf{r}^3_{I,d}$ of the camera and induces a disturbance motion p_0 by manipulating the suspension of the platform by hand. Due to the mechanical constraints of the suspension, the induced motion is given by the measured dof ϕ and ψ, see Fig. 8a). The angular velocities $\tilde{\boldsymbol{\omega}}^{I0}_0$ of p_0 and the measured accelerations $\tilde{\mathbf{a}}^{I0}_0$ obtained by IMU0 are depicted in Fig. 8b)-c). Here it can be seen that the large acceleration in x-direction is due to gravity and the acceleration in y-direction corresponds to the centrifugal acceleration due to the motion of the suspension. The desired orientation $\mathbf{r}^3_{I,d}$ is defined by integration of the angular velocities $\boldsymbol{\omega}^{I3}_{3,d}$ given in Fig. 8d) and the initial orientation $\mathbf{r}^3_{I,d,0} = [\cos(45°), 0, \sin(45°, 0)]^T$, cf. (10).

To suppress the motion of p_0 and obtain the desired orientation $\mathbf{r}^3_{I,d}$ of the camera, the control input $\boldsymbol{\tau}_a$ depicted in Fig. 9a) is calculated by the control strategy. The resulting motion of the actuated dof $\mathbf{q}$ is given in Fig. 9b).

The control error $\mathbf{e}_r$ shown in Fig. 10a) accounts for the error between the desired orientation $\mathbf{r}^3_{I,d}$ and the estimated orientation $\mathbf{r}^3_I$. It can be seen that a very good tracking accuracy is obtained by the proposed control strategy. The overall orientation error of the camera, however, is increased by the error of the attitude estimation strategy. The measurements of the angles of the suspension ϕ and ψ allow to calculate the actual orientation $\mathbf{r}^3_I$ of the camera in the experimental setup, by using $\theta = 90°$ and the encoder measurements $\mathbf{q}$ in (5). Thus, the overall attitude error $\mathbf{r}^3_{I,d} - \mathbf{r}^3_I$ of the camera can be calculated and parameterized by the angles α, β and γ, see Fig. 10 b).

To evaluate the attitude estimation error of p_0, Fig. 10 c) shows a comparison of the measured angles ϕ, ψ and θ of the suspension with the corresponding estimated values. It is evident from this figure that the overall attitude error of the camera is largely influenced by the error of the attitude estimation strategy. In

Post-print version of the article: F. Königseder, W. Kemmetmüller, and A. Kugi, “Attitude control strategy for a camera stabilization platform”, *Mechatronics*, vol. 46, pp. 60–69, 2017. DOI: 10.1016/j.mechatronics.2017.06.012
The content of this post-print version is identical to the published paper but without the publisher’s final layout or copy editing.

particular, the slow drift in γ results from the drift of the attitude estimation in this axis, cf. the drift of ψ in Fig. 10 c). As the axis of rotation of γ points into the vertical direction in this experiment, this drift is explained by a bias error of the gyroscopes in the IMU. It is discussed in detail in [1] that this drift cannot be completely eliminated by the given sensor setup due to a lack of measurement information around this axis. A slow drift does not constitute a major problem in the given application, since typically no static scene is filmed and it can be easily compensated by the camera operator by changing $\mathbf{r}^3_{I,d}$. It is far more important from a practical point of view (i.e. filming of a dynamic scene) that there are no significant fast motions in the camera attitude. Fig. 10 b) confirms that the combination of the proposed control concept and the attitude estimation of [1] gives very good results in this respect. This is also confirmed by the error between the desired angular velocity $\boldsymbol{\omega}^{I3}_{3,d}$ of the camera and the angular velocity $\tilde{\boldsymbol{\omega}}^{I3}_{3}$ measured by IMU3 depicted in Fig. 10 d), which lies in the range of the measurement accuracy of IMU3.

6. Conclusions

In this paper, a control strategy for the attitude control of a portable inertially stabilized platform (ISP) for film and broadcast cameras was proposed. The presented control strategy provides an alignment of the camera with a desired orientation such that movements of the operator who carries the ISP do not distract the line of sight of the camera. At the same time, the desired orientation of the camera can be changed by the operator. The control strategy is based on an attitude estimation of the camera orientation presented in [1], which uses the measurements of two inertial measurement units (IMU). The specific placement of the two IMUs on the handle and the camera mounting point of the ISP is beneficial for the presented control strategy. The control concept combines a feedforward compensation of the induced disturbances and a feedback control of the deviation of the attitude. It systematically takes into account the (nonlinear) dynamics of the overall (multi-body) system, which, up to the authors' knowledge, has not been utilized for the attitude stabilization problem by gimbaled platforms so far. Simulation and experimental results show the advantage of taking into account both a feedforward and feedback part in the control strategy. In conclusion, the attitude stabilization concept shows a significant improvement in comparison to existing solutions. Currently, the results of the prototype system are transferred to obtain a commercially feasible system.

Acknowledgement

This work was supported by the Austrian Research Promotion Agency (FFG), Grant No.: 827482.

Post-print version of the article: F. Königseder, W. Kemmetmüller, and A. Kugi, "Attitude control strategy for a camera stabilization platform", *Mechatronics*, vol. 46, pp. 60–69, 2017. DOI: 10.1016/j.mechatronics.2017.06.012
The content of this post-print version is identical to the published paper but without the publisher's final layout or copy editing.

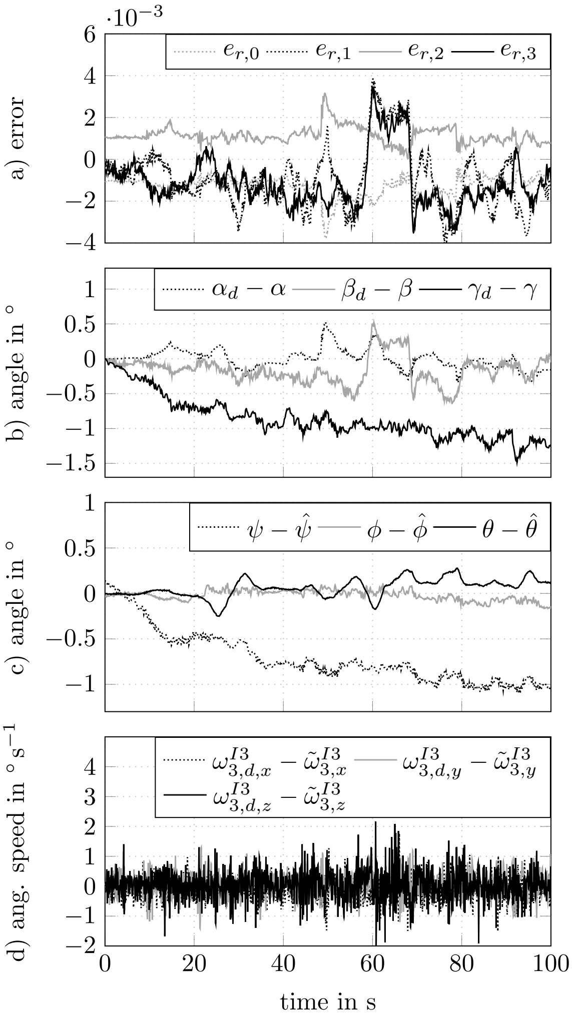

Figure 10: Experimental results: a) orientation error $\mathbf{e}_r$, b) corresponding error in the angles, c) estimation error of inertial measurement for $\mathbf{r}^0_I$ and, d) error of angular speed $\boldsymbol{\omega}^{I3}_3$.

Post-print version of the article: F. Königseder, W. Kemmetmüller, and A. Kugi, "Attitude control strategy for a camera stabilization platform", *Mechatronics*, vol. 46, pp. 60–69, 2017. DOI: 10.1016/j.mechatronics.2017.06.012
The content of this post-print version is identical to the published paper but without the publisher's final layout or copy editing.

References

[1] F. Königseder, W. Kemmetmüller, A. Kugi, Attitude estimation using redundant inertial measurement units for the control of a camera stabilization platform, IEEE Transactions on Control Systems Technology 24 (5) (2016) 1837–1844.

[2] T. L. Vincent, Stabilization for film and broadcast camera [application of control], IEEE Control Systems Magazine 28 (1) (2008) 20–25.

[3] G. Mercado, The filmmaker's eye: learning (and breaking) the rules of cinematic composition, Focal Press, Boston, USA, 2013.

[4] L. W. H. Jerry Holway, Steadicam Operator's Handbook, Focal Press, Boston, USA, 2009.

[5] T. W. Kenyon, Stabilizer for sighting devices, patent: US2811042, 1957.

[6] M. K. Masten, Inertially stabilized platforms for optical imaging systems, IEEE Control Systems Magazine 28 (1) (2008) 47–64.

[7] H. Helble, S. Cameron, OATS: Oxford aerial tracking system, Robotics and Autonomous Systems 55 (9) (2007) 661–666.

[8] Z. Hurak, M. Rezac, Image-based pointing and tracking for inertially stabilized airborne camera platform, IEEE Transactions on Control Systems Technology 20 (5) (2012) 1146–1159.

[9] J. Debruin, Control systems for mobile satcom antennas, IEEE Control Systems Magazine 28 (1) (2008) 86–101.

[10] M. N. Soltani, R. Izadi-Zamanabadi, R. Wisniewski, Reliable control of ship-mounted satellite tracking antenna, IEEE Transactions on Control Systems Technology 19 (1) (2011) 221–228.

[11] J. M. Hilkert, Inertially stabilized platform technology, IEEE Control Systems Magazine 28 (1) (2008) 26–46.

[12] A. Rue, Precision stabilization systems, IEEE Transactions on Aerospace and Electronic Systems AES-10 (1) (1974) 34–42.

[13] S. Hong, K. D. Cho, Kinematic algorithms and robust controller design for inertially stabilized system, IEEE Transactions on Mechatronics 19 (1) (2014) 76–87.

[14] F. R. Rubio, M. G. Ortega, F. Gordillo, M. Vargas, Application of position and inertial-rate control to a 2-DOF gyroscopic platform, Robotics and Computer-Integrated Manufacturing 26 (4) (2010) 344–353.

[15] J. T.-Y. Wen, K. Kreutz-Delgado, The attitude control problem, IEEE Transactions on Automatic Control 36 (20) (1991) 1148–1162.

[16] M. S. Grewal, L. R. Weill, A. P. Andrews, Global Positioning Systems, Inertial navigation, and Integration, Wiley, Hoboken, USA, 2007.

[17] A. Tayebi, S. McGilvray, Attitude stabilization of a vtol quadrotor aircraft, IEEE Transactions on Control Systems Technology 14 (3) (2006) 562–571.

[18] R. Kristiansen, P. J. Nicklasson, J. Gravdahl, Satellite attitude control by quaternion-based backstepping, IEEE Transactions on Control Systems Technology 17 (1) (2009) 227–232.

[19] C. G. Mayhew, R. G. Sanfelice, A. R. Teel, Quaternion-based hybrid control for robust global attitude tracking, IEEE Transactions on Automatic Control 56 (22) (2011) 2555–2566.

[20] F. Lizarralde, J. T. Wen, Attitude control without angular velocity measurement: a passivity approach, in: Proceedings of the 1995 IEEE International Conference on Robotics and Automation, Vol. 3, Nagoyo, JP, 1995, pp. 2701–2706.

[21] P. J. Kennedy, R. L. Kennedy, Direct versus indirect line of sight (LOS) stabilization, IEEE Transactions on Control Systems Technology 11 (1) (2003) 3–15.

[22] M. W. Dunnigan, C. M. Wronka, Comparison of control techniques for a robotic manipulator with base disturbances, IET Control Theory and Applications 5 (8) (2011) 999–1012.

[23] R. Murray, S. Sastry, Z. Li, A Mathematical Introduction to Robotic Manipulation, CRC Press, Boca Raton, USA, 1994.

[24] M. Spong, M. Vidyasagar, Robot Dynamics and Control, John Wiley and Sons, Hoboken, USA, 1989.

[25] Analog Devices, ADIS16480, datasheet, online: http://www.analog.com, visited in Dec. 2016.

[26] Analog Devices, ADIS16485, datasheet, online: http://www.analog.com, visited in Dec. 2016.

Post-print version of the article: F. Königseder, W. Kemmetmüller, and A. Kugi, "Attitude control strategy for a camera stabilization platform", *Mechatronics*, vol. 46, pp. 60–69, 2017. DOI: 10.1016/j.mechatronics.2017.06.012
The content of this post-print version is identical to the published paper but without the publisher's final layout or copy editing.

[27] J. B. Kuipers, Quaternions and Rotation Sequences: A Primer with Applications to Orbits, Aerospace, and Virtual Reality, Princeton University Press, Princeton, USA, 2002.

[28] M. D. Shuster, A survey of attitude representations, The Journal of the Astronautical Sciences 41 (4) (1993) 439–517.

[29] C. Wronka, M. Dunnigan, Derivation and analysis of a dynamic model of a robotic manipulator on a moving base, Robotics and Autonomous Systems 59 (10) (2011) 758 – 769.

[30] P. J. From, V. Duindam, J. T. Gravdahl, S. Sastry, Modeling and motion planning for mechanisms on a non-inertial base, in: Proceedings of the 2009 IEEE International Conference on Robotics and Automation (ICRA 09), Kobe, JP, 2009, pp. 3320–3326.

[31] S. Andersson, A. Söderberg, S. Björklund, Friction models for sliding dry, boundary and mixed lubricated contacts, Tribology International 40 (4) (2007) 580–587.

[32] C. Makkar, W. E. Dixon, W. G. Sawyer, G. Hu, A new continuously differentiable friction model for control systems design, in: Proceedings of the 2005 IEEE/ASME International Conference on Advanced Intelligent Mechatronics, Monterey, USA, 2005, pp. 600–605.

[33] C. Abdallah, D. M. Dawson, P. Dorato, M. Jamshidi, Survey of robust control for rigid robots, IEEE Control Systems 11 (2) (1991) 24–30.

[34] M. Spong, M. Vidyasagar, Robust linear compensator design for nonlinear robotic control, IEEE Journal on Robotics and Automation 3 (4) (1987) 345–351.

[35] Z. Qu, J. F. Dorsey, X. Zhang, D. M. Dawson, Robust control of robots by the computed torque law, Systems and Control Letters 16 (1) (1991) 25 – 32.

[36] M. S. Fadali, E. Yaz, Stability robustness and robustification of the exact linearization method of robotic manipulator control, in: Proceedings of the 34th IEEE Conference on Decision and Control, Vol. 2, New Orleans, USA, 1995, pp. 1624–1629.

[37] S. B. Niku, Introduction to Robotics, John Wiley and Sons, Hoboken, USA, 2010.

Post-print version of the article: F. Königseder, W. Kemmetmüller, and A. Kugi, "Attitude control strategy for a camera stabilization platform", *Mechatronics*, vol. 46, pp. 60–69, 2017. DOI: 10.1016/j.mechatronics.2017.06.012